Tectonics®

RESEARCH ARTICLE
10.1029/2024TC008721

Development of Intra-Rift Basins During Stress Field Change in the Central Upper Rhine Graben (SW Germany)

Florian Bauer[1], **Jens C. Grimmer**[1], **Lars Houpt**[1], **Thomas Hertweck**[1], **and Eva Schill**[2]

[1]Karlsruhe Institute of Technology, Karlsruhe, Germany, [2]Lawrence Berkeley National Laboratory, Berkeley, CA, USA

Key Points:

- Development of new intra-rift basin generation superposing on early syn-rift basins
- Orientation of intra-rift basins in the Upper Rhine Graben controlled by shallow rooted faults, nucleated in graben fill strata of 32–28 Ma
- Intra-rift basin formation linked to a stress field change at 27 ± 1 Ma

Correspondence to:

J. C. Grimmer,
jens.grimmer@kit.edu

Citation:

Bauer, F., Grimmer, J. C., Houpt, L., Hertweck, T., & Schill, E. (2025). Development of intra-rift basins during stress field change in the central Upper Rhine Graben (SW Germany). *Tectonics*, *44*, e2024TC008721. https://doi.org/10.1029/2024TC008721

Received 9 NOV 2024
Accepted 22 MAR 2025

Author Contributions:

Conceptualization: Jens C. Grimmer, Eva Schill
Data curation: Florian Bauer, Lars Houpt, Thomas Hertweck
Formal analysis: Lars Houpt, Thomas Hertweck
Funding acquisition: Eva Schill
Investigation: Florian Bauer, Jens C. Grimmer
Methodology: Florian Bauer, Jens C. Grimmer, Lars Houpt, Thomas Hertweck, Eva Schill
Project administration: Florian Bauer
Software: Florian Bauer, Lars Houpt, Thomas Hertweck
Supervision: Jens C. Grimmer, Eva Schill
Validation: Florian Bauer, Jens C. Grimmer, Lars Houpt, Thomas Hertweck
Visualization: Florian Bauer, Jens C. Grimmer, Lars Houpt, Thomas Hertweck
Writing – original draft: Florian Bauer, Jens C. Grimmer, Lars Houpt, Thomas Hertweck

Abstract The essentially non-magmatic continental rift system of the Upper Rhine Graben (URG) is segmented and characterized by intra-rift sub-basins that exhibit NE to NW trends suggesting complex basin development during rifting. Structural modeling and analyses of an about 40 km^2 3D seismic survey from the northern part of the central URG segment show deep rooted NNE-striking faults controlling early, syn-rift 1, extensional basin evolution from about 47 Ma to 27 Ma. The change in stress field at about 27 Ma and subsequent reactivation of these deep rooted basement faults resulted in a new set of shallow rooted en-echelon faults. On a larger scale this change in stress field was accompanied by a shift of regional depocenters. The shallow rooted en-echelon faults nucleated in 32–28 Ma old strata and are linked by conjugated relay ramps that control the development of latest Oligocene to early Miocene syn-rift 2 basins trending N to NNW. Although we only studied a small part of the >11,000 km^2 large URG, we hypothesize that this type of intra-rift basin development in the hanging wall of major deep rooted normal faults is more widespread in the graben and may represent a general style for the development of other late Oligocene-early Miocene intra-rift basins, such as for example, the distinct Heidelberg Basin. We suggest increasing mechanical coupling between the European lower plate and Adriatic upper plate at c. 30 Ma to 28 Ma as a possible cause for the Oligocene stress field change.

Plain Language Summary The URG is a c. 300 km long, 30–40 km wide, essentially non-magmatic continental rift. Rifts are longitudinal areas where the Earth's crust extends. Extension generates subsidence where sediments can accumulate to form sedimentary basins. Deformation of these rifts is strongly controlled by rift-external forces (or the regional stress field), expressed for example, by the occurrence of minor earthquakes. Extension generates with time multiple local basins within the entire rift. Therefore they are named intra-rift basins. These intra-rift basins are filled up with sediments during their formation and can be associated with resources such as geothermal fluids or hydrocarbons. Sedimentary thicknesses, orientation and distribution of these basins therefore provide information on the structural development of the entire rift and help to better understand fluid flow in the rift and to explore and exploit energy resources.

1. Introduction

1.1. Intra-Rift Basins

Continental rifts consist of several intra-rift sub-basins resulting from several interfering geological boundary conditions that need to be deciphered to understand cause and effect during rift development (e.g., Withjack et al., 2002). Numerical and analog modeling has shown that basin formation in orthogonal rifts occurs mainly within rift-parallel sub-basins, whereas basin development in oblique rifts is more complicated and appears to be controlled by the obliquity between regional extension and rift boundary faults (e.g., Agostini et al., 2009; Brune, 2014). In the East African rift system inherited lithospheric and crustal scale structures and anisotropies control segmentation as well as intra-rift basin formation and distribution (Brune et al., 2017; Corti et al., 2007; Ring, 1994; Samsu et al., 2023). A change of extension direction and its impact on structural development due to external plate tectonic rearrangements was discussed for example, for the Rio Grande Rift, the Kenyan rift, and the Red Sea rift system (Bosworth et al., 2005; Golombek et al., 1983; Strecker et al., 1990). Minor and major stress field changes have been proposed, but not yet well constrained in time for the URG (e.g., Schumacher, 2002). For the URG reactivation of late Variscan lithospheric shear zones and the inheritance of other crustal structures are proposed to have influenced its segmentation and cross-sectional asymmetry (Grimmer et al., 2017; Schumacher, 2002). Late Variscan, W-dipping mylonitic-cataclastic shear zones in the basement of the eastern rift shoulder comprise lithospheric-scale mechanical anisotropies that have localized the URG, and NE- to NW-striking upper crustal fault zones of Permo-Carboniferous and Mesozoic age continue to influence

Writing – review & editing:
Florian Bauer, Jens C. Grimmer, Lars Houpt, Thomas Hertweck, Eva Schill

neotectonic deformation and seismic section properties along the URG (Grimmer et al., 2017). Intra-rift basins of different sizes, orientations and geometries were identified on the basis of numerous borehole and 2D seismic data (e.g., GeORG-Projektteam, 2013; Schad, 1964; Wirth, 1962). We reprocessed, analyzed and re-interpreted a c. 40 km^2 area within the 279 km^2 Karlsruhe-Nord 3D seismic survey, which was originally designed for industrial oil and gas exploration. In order to obtain a consistent structural model, the seismic-to-well ties and formation top correlations were re-evaluated using borehole data. Since the Cenozoic strata can be very well imaged by the seismic data, this study focuses on the development of intra-rift basins in the central URG. The understanding of the development of intra-rift basins helps to decipher the complex structural geometries in the URG.

1.2. Regional Geology

The NNE-striking URG (Figure 1) developed from about 47 Ma as a response to changing lithospheric stresses in the northwestern Alpine foreland. The c. 300 km long and 30–40 km wide URG is part of the European Cenozoic Rift System, which extends for about 1,000 km from the North Sea to the Mediterranean Sea (Figure 1) and is bound to the N and S by accommodation zones that separate the URG from the Rhenish Massif and the Lower Rhine Graben in the NW and the Bresse-Rhone Graben in the SW (Figure 1). The URG is internally subdivided by accommodation zones into southern, central and northern segments (Grimmer et al., 2017). The accumulated Cenozoic sediments, including up to 350 m of Quaternary successions, comprise up to 3,500 m thick, predominantly low-energy sedimentary successions in the URG (e.g., Berger et al., 2005; Böcker et al., 2017). Due to a slight SSE tilting and very gentle pre-Cenozoic shortening, the stratigraphic age of the URG subcrop decreases southward (Böcker et al., 2017; Lutz & Cleintuar, 1991). The estimated total extension in the URG is 7%–18% (Grimmer et al., 2017). As typical for narrow, non-magmatic rifts with less than 21% total extension, the normal fault segments in the URG are linked by relay ramps and not transfer faults (Acocella et al., 2005; Reinhold et al., 2016).

Along the NE-SW-striking Erstein-Renchen zone, the URG floor drops down by >1,500 m in the central segment. Along the several-km-wide Ludwigshafen zone, the URG floor of the northern segment drops down by further c. 500 m, which is mainly due to development of the Heidelberg basin (Figure 1). This basin represents the largest and most pronounced Neogene intra-rift basin of the URG. In the northern part of the central segment of the URG, N- to NNE-striking normal faults such as the Leopoldshafen and Stutensee faults interact with (N)NW-striking normal faults (Figure 1). These faults may be interpreted as southeasternmost segments of the NNW-trending Ludwigshafen hinge zone (Figure 1).

The development of the URG succeeded a phase of Late Cretaceous and Eocene dynamic topography and associated volcanism of the Southern Central European Volcanic Province (Binder et al., 2023). Late Cretaceous to Eocene uplift caused erosion of large parts of the Mesozoic successions in the northern URG area (Böcker et al., 2017; Eynatten et al., 2021; Lutz & Cleintuar, 1991). The early Eocene-Oligocene successions were deposited during a regional (W)NW extension and the formation of large NE to NNE-trending depocenters in the southern and central segments (e.g., Strasbourg-Rastatt Basin; Figure 1). During Neogene (E)NE extension, the main rift-basin scale depocenter shifted to the NNW-trending Heidelberg Basin (e.g., Grimmer et al., 2017). In SW Germany and adjacent NE France, subordinate primitive alkaline volcanism occurred between about 27 Ma to 9 Ma (Binder et al., 2023). Major volcanic activity in the URG occurred between about 18 Ma and 14 Ma in the Kaiserstuhl and Vogelsberg areas (Figure 1), accompanied by a phase of dynamic topography and an uplift of c. 1,000 m in the southern URG (Vosges-Black Forest dome; Binder et al., 2023; Grimmer et al., 2017). Miocene uplift led to a partial erosion of earlier rift-filling sedimentary sequences in the southern and central segments and to a generally well-documented angular unconformity at the base of Pliocene-Quaternary strata (e.g., Geyer et al., 2011), except for the Neogene depositional center of the Heidelberg Basin, where 2D seismic lines yet do not exhibit a well-defined angular unconformity (Gabriel et al., 2013). This rift-wide unconformity is overlain by variable Pliocene to Holocene fluvial and (minor) eolian sediments, which generally plunge NNE-ward in the study area. These post-Miocene sediments were probably deposited during cooling-induced subsidence following the Miocene dynamic topography (Binder et al., 2023). The NNE-trending Strasbourg-Rastatt basin is a major axial intra-rift basin, which is bound to the north by NNW-striking faults of the Ludwigshafen zone (Figure 1). This zone marks the several km wide western boundary of the N- to NNW-trending Heidelberg basin, which is characterized by a marked increase of Quaternary to Neogene thicknesses toward ESE (Kärcher, 1987; Schad, 1964). It separates the clearly subsiding eastern from only weakly subsiding or even weakly uplifting western areas (Fuhrmann et al., 2015; Mälzer, 1988).

10.1029/2024TC008721

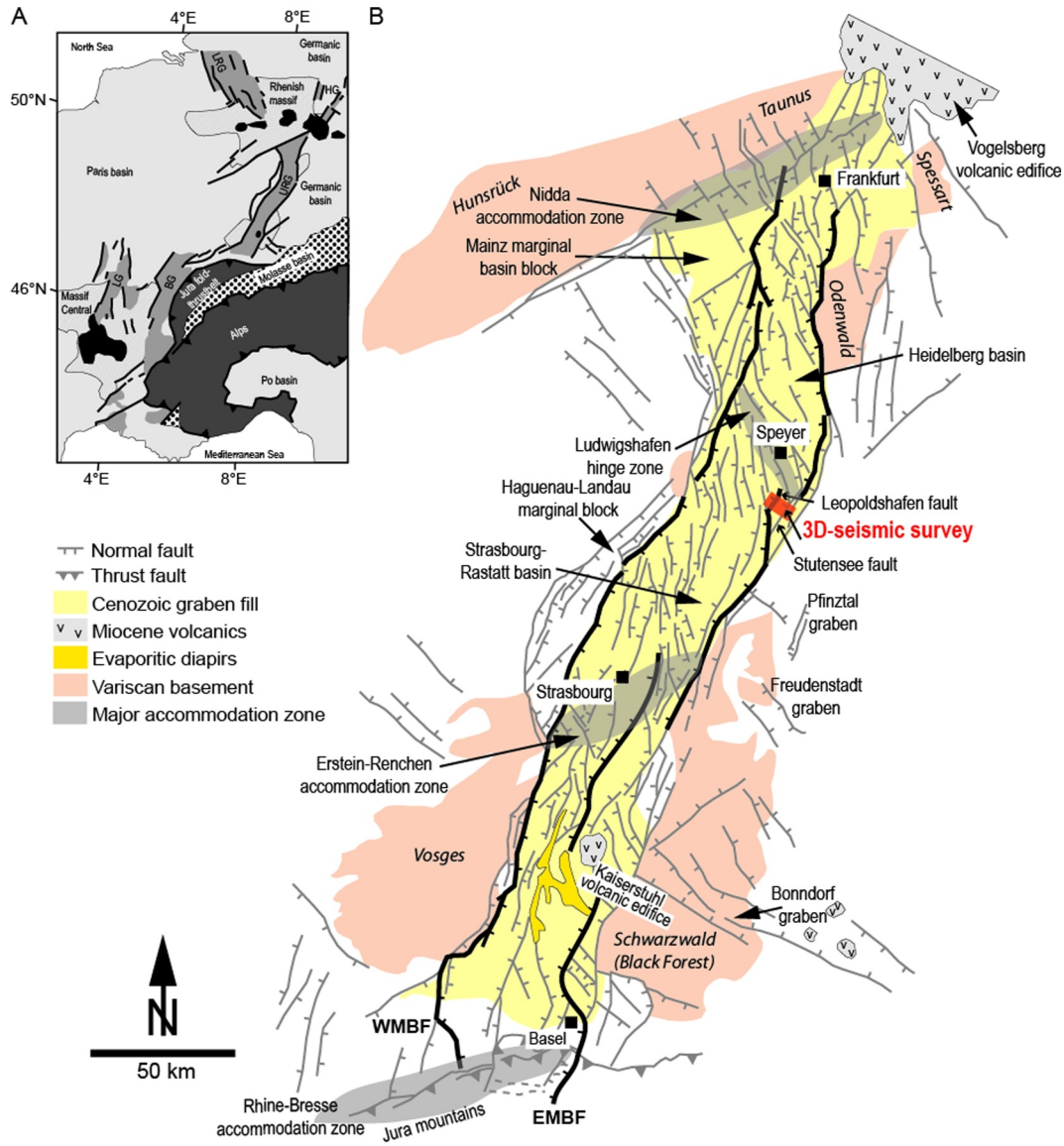

Figure 1. (a) Inset map showing the Upper Rhine Graben (URG) as part of the European Cenozoic Rift System (ECRIS) including the Lower Rhine Graben (LRG), Hessian Graben (HG), Burgundy Graben (BG), Limagne Graben (LG) in the context of major tectonic units mentioned in the text. Black units mark major Cenozoic volcanic units. (b) Overview of the main structural units of the URG (modified from Grimmer et al. (2017)) and the location of 3D-seismic survey of this study and the Stutensee and Leopoldshafen faults. EMBF, Eastern Main Boundary Fault; WMBF, Western Main Boundary Fault.

The stratigraphy of the central URG is displayed in Figure 2. Eocene to Oligocene fluvio-lacustrine to brackish-marine sedimentary sequences form the main early syn-rift sequences, the Haguenau and Pechelbronn Formations (Fm.) and occur in all segments of the URG, with the southern and central segments forming major depocenters (Derer et al., 2005; Grimm et al., 2011). The Haguenau Formation consists of lacustrine clays and marls, intercalated with evaporites of the Wittelsheim Formation. In the southern segment, these layers form thick halite successions with intercalated potash salt seams (e.g., Esslinger, 1976). The clastic material of the Pechelbronn Fm. originates mainly from the northern part of the URG in the area of today's Mainz marginal basin block (Figure 1; "Mainz Basin"), where drilled sandstones and conglomerates constitute a well-documented alluvial fan (e.g., Reinhold et al., 2016). The peak of the flooding and associated deposition of marine sediments in the URG took place during the Rupelian transgression. This resulted in the c. 20–45 m thick Foraminifera marls, overlain by the up to 20 m thick Fish Shale ("Rupel clay"). This "Rupel Clay" forms the basal units of the Froidefontaine Fm. and the most important, basin-wide seismic reflector in the URG (e.g., Rotstein et al., 2005). The

10.1029/2024TC008721

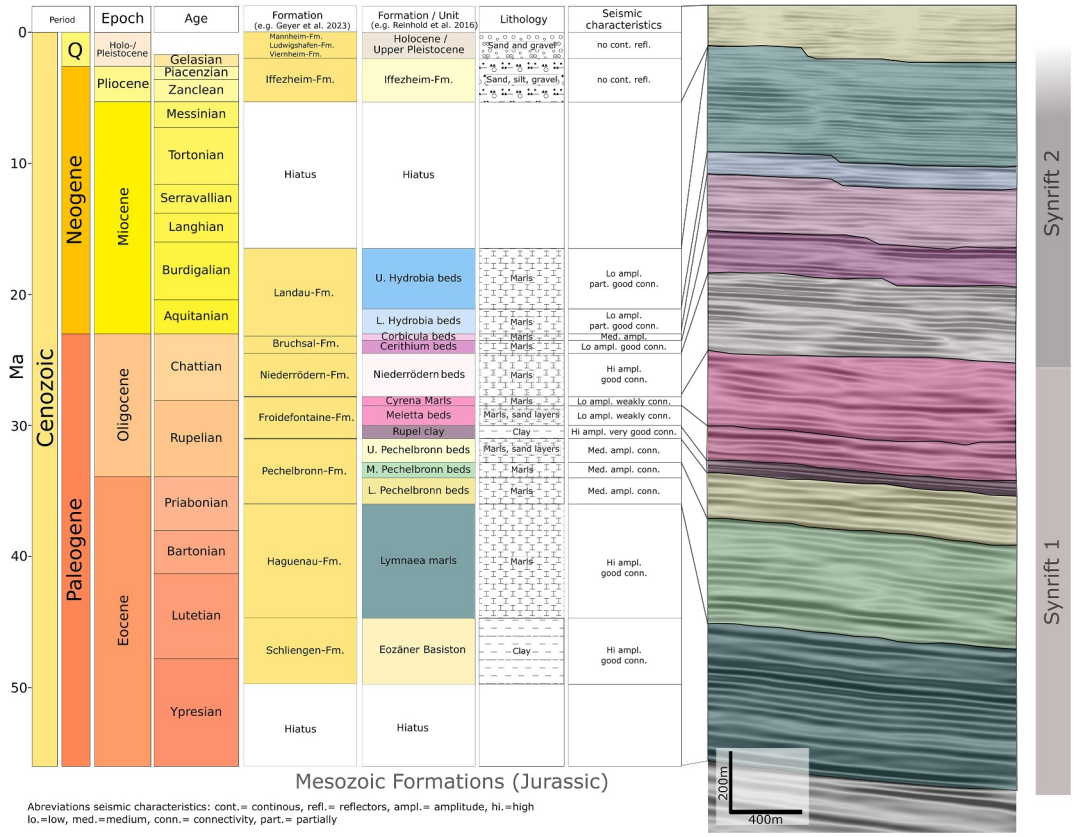

Figure 2. Stratigraphic units, lithological representation and seismic characteristics of the Neogene and Paleogene sedimentary sequences in the study area. The transition between syn-rift 1 and syn-rift 2 successions marks a change of the regional stress field as outlined in the text. Stratigraphy is compiled from Reinhold et al. (2016), Geyer et al. (2011), and Grimm et al. (2011).

Froidefontaine Fm. (or Gray Bed Series, e.g., Wirth, 1962) consists of uniform, mica-bearing gray marls and centimeter to several meter thick sand layers (Geyer et al., 2011). The Froidefontaine Fm. comprises two Rupelian transgression cycles and was an important target of hydrocarbon exploration in the URG due to the presence of sand layers and lenses (Böcker et al., 2017; Pirkenseer et al., 2013; Reinhold et al., 2016). The subsequent Chattian regression marks the transition from marine (Meletta beds) to brackish (Cyrena marl) to fluviatile deposits of fine-grained siliciclastics and marls of the uppermost Oligocene Niederrödern Fm. The Oligocene-Miocene boundary at 23 Ma lies within the Bruchsal Fm., comprising carbonates with minor sand layers (Cerithia beds) and uniform thin layers of alternating light limestone laminae and dark gray marls with locally significant evaporite thicknesses (Corbicula beds; Geyer et al., 2011). The Landau Fm. comprises brackish-marine, early Miocene (Aquitanian-Burdigalian) dolomite-shale interlayers of the Lower and Upper Hydrobia beds, deposited during the Burdigalian transgression at about 18–20 Ma (Geyer et al., 2011; Grimm et al., 2011). The weakly to unconsolidated Pliocene to Quaternary fluvio-lacustrine silt-sand-gravel successions are usually summarized as one unit in seismic studies and are therefore stratigraphically not further differentiated here.

2. Materials and Methods

2.1. 3D Seismic Data

The seismic data used for this study comprise c. 40 km^2 of a 279 km^2 large survey conducted from January to May 2012. Here we present a subset of a c. 10 km × 4 km rectangular area around the Campus North of the Karlsruhe Institute of Technology (KIT-Campus North; Figure 1). The complete 3D Vibroseis data set was acquired using a standard design with receiver lines (inlines) oriented from WNW to ESE (115° azimuth, subparallel to the main tectonic strike) and orthogonal source lines (crosslines). In the subset, source point and line intervals are 40 and

400 m respectively. A variable receiver line spacing of 400 and 200 m in the western and eastern parts, respectively, and a maximum offset of 3,800 m were used. The bin size is 20 m × 20 m. This has resulted in a nominal fold of 42 in the west and 70 in the east. A sweep in the frequency range of 12–96 Hz was used as the source signal by the three vibrators with six sweeps per shot point.

Prior to migration, a standard land processing sequence was applied to the data, including surface-consistent and adaptive spiking deconvolution, flex-binning, static corrections, velocity analysis and normal-moveout (NMO) correction, bandpass filtering and automatic gain control to suppress strong noise bursts, before dip moveout (DMO) correction and stacking. Finally, a layer-based and global tomographic approach was used to determine an interval velocity model and a vertically transverse isotropic Kirchhoff pre-stack depth migration was performed. Well information was used to control the quality of the velocity field and was included in the initial anisotropy model. A residual moveout correction was applied before stacking the data. Finally, FXY deconvolution and a time-variant bandpass filter helped to improve the signal-to-noise ratio of the image. The subset consists of two 3D cubes that were migrated in time after stacking and in depth before stacking. Both cubes are fully 3D-migrated using all available data from the large survey. This processing resulted in the visualization of reflectors with a good signal-to-noise ratio down to a depth of about 3 km depth revealing consistent sedimentary layering. Around regional faults, especially in the footwall, a significant fault shadow of low consistency is developed. The depth migration is zero-phase and follows the reverse SEG standard polarity convention. The Kirchhoff migration requires a smooth velocity model. Areas with strong velocity contrasts, as observed along the main fault systems in our data set, can lead to a degradation in imaging quality around and beneath these areas. The resolution of the seismic data can be estimated from the wavelength (Kallweit & Wood, 1982). With a dominant frequency of about 40 Hz on target depth and using the interval velocities from the migration model, we can estimate a vertical resolution limit of approximately 20 m. At lower layer thicknesses, reflections from the top and bottom of the layer are no longer be fully separated and tuning effects occur, making the determination of layer thicknesses in general increasingly erroneous, especially for areas with lower signal-to-noise ratios. Therefore layers, for which borehole data indicate thicknesses of less than 20 m, can no longer fully separated.

2.2. Borehole Data

The investigated 3D seismic area includes 21 in-field and 12 offset wells, within 5 km away from the study area with depths of more than 1,000 m. As hydrocarbons were trapped in slightly tilted sand layers in the footwall of the Leopoldshafen fault the majority of drill sites occur immediately W of this fault (Figure 6; Wirth, 1962). Most of the wells, drilled from the late 1950s to the early 1980s, intersected Cenozoic formations down to the Froidefontaine Fm., but few also intersected the Lymnaea marls (Haguenau Fm.). One in-field well and three offset wells also intersected Mesozoic formations, generally middle Jurassic to late Triassic rocks, with the deepest in-field well intersecting the early Triassic Buntsandstein Group at approximately 2.9 km depth. The stratigraphic identification and boundaries were taken from drilling reports. We re-evaluated and partly reinterpreted the log data for stratigraphic assignment as described below. To create the 3D geological model, the information on the depth of stratigraphic changes was treated as fixed points. The general approach for establishing stratigraphic boundaries included macroscopic petrographic analysis of drill cuttings, micropaleontological determinations, and correlation with borehole geophysical logs. Their uncertainties, though not precisely quantifiable due to the relatively dated nature of the data, are estimated to be within a few meters.

2.3. Structural Modeling

The geological structural model was created using Petrel software, version 2020. The Structural Framework Workflow, based on interpreted seismic horizons, was utilized for model construction. The lateral extent of the model corresponds to the seismic data, reduced at the western and eastern marginal parts due to edge distortions in the seismic data. At its upper boundary, the model is defined by the digital elevation model derived from SRTM data (NASA JPL, 2013). At depth, the 3D structural model terminates at the base of the Cenozoic sediments.

For the 3D geological model, 12 seismic reflectors were mapped as marker horizons and characterized using borehole information and seismic attribute analyses. Nine of these reflectors occur in the entire study area. Three reflectors could not be clearly identified in the Eastern block due to discontinuities and lack of borehole data.

The faults were identified by displacements of the reflectors and, in a second step, supported by attribute analyses. For the latter, a gradient structure tensor attribute (Randen et al., 2000) was calculated and analyzed (Figure 3). In

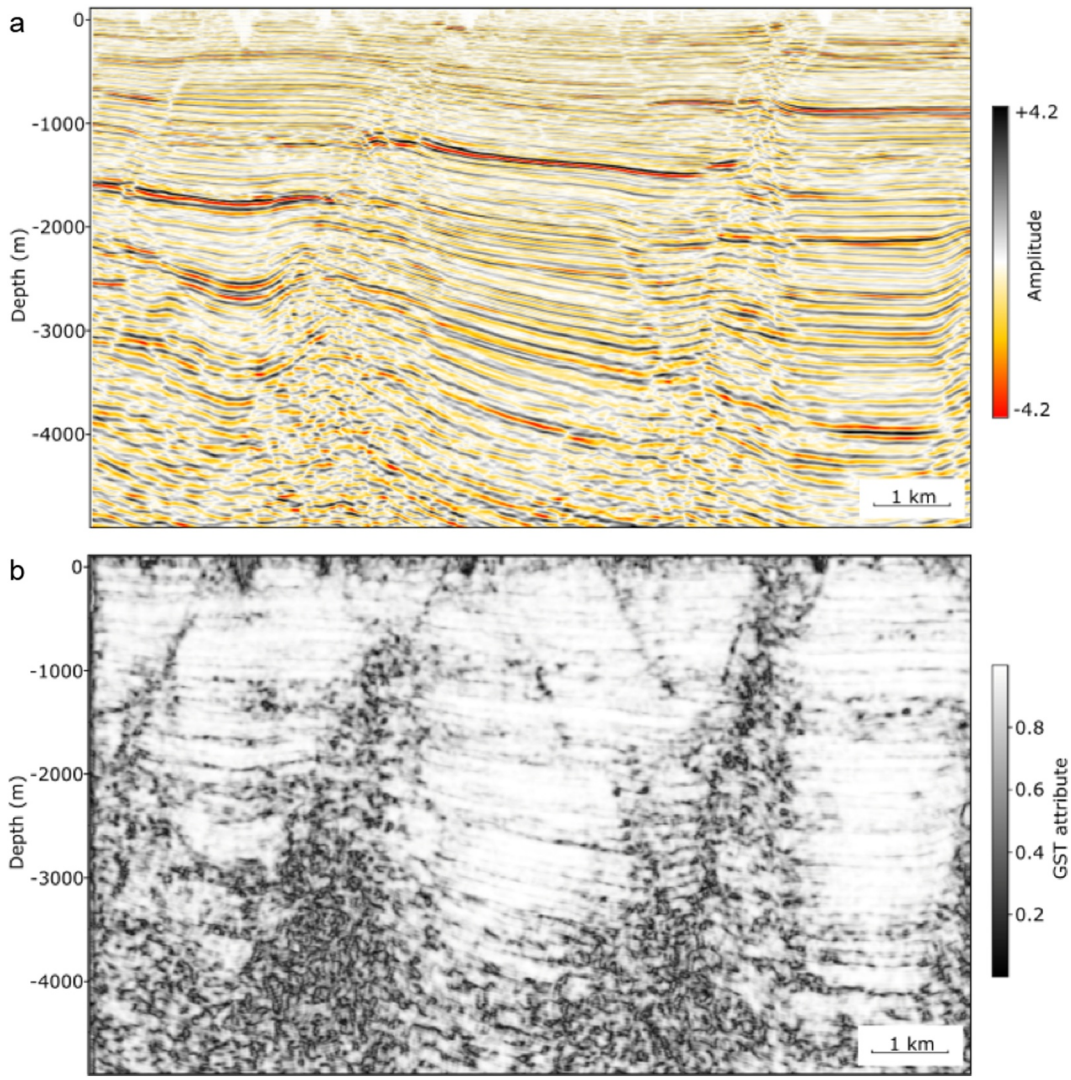

Figure 3. (a) Inline from the depth-migrated volume and (b) corresponding inline from the gradient structure tensor attribute volume. The attribute clearly displays the two major deep rooted Leopoldshafen and Stutensee faults in the area and several minor, shallow rooted faults, which are not readily observable in the main seismic data.

most cases, inlines were used and the digitization was performed in 3D with a resolution of five inlines. The thickness distributions of sedimentary strata are analyzed by isopach maps and displayed by violin plots. Stratigraphic classification was based on biostratigraphic and lithostratigraphic evaluations of drill cuttings. Stratigraphic information from drilling reports and seismic-to-well ties were re-evaluated using electric resistivity (RES) and self-potential (SP) logs from borehole data.

3. Data and Results

3.1. Stratigraphy and Seismic Characterization of Reflectors

Three unconformities can be identified in the graben filling: base Cenozoic, base Niederrödern Fm. and base Pliocene. Two basin-scale regional unconformities are readily identified and documented elsewhere (e.g., Rotstein et al., 2005): the angular unconformity of the base of the Cenozoic representing the lower model boundary of this study and the base of the Pliocene. The Oligocene unconformity has not yet been documented as a rift basin scale unconformity. The base of the Cenozoic includes a hiatus of more than 100 million years between the low-amplitude and low-continuity reflectors of the Jurassic successions and the well-defined, continuous reflectors of the Haguenau Fm. (Lymnaea Marls). The Haguenau Fm. and the Pechelbronn Fm. contain several reflectors used

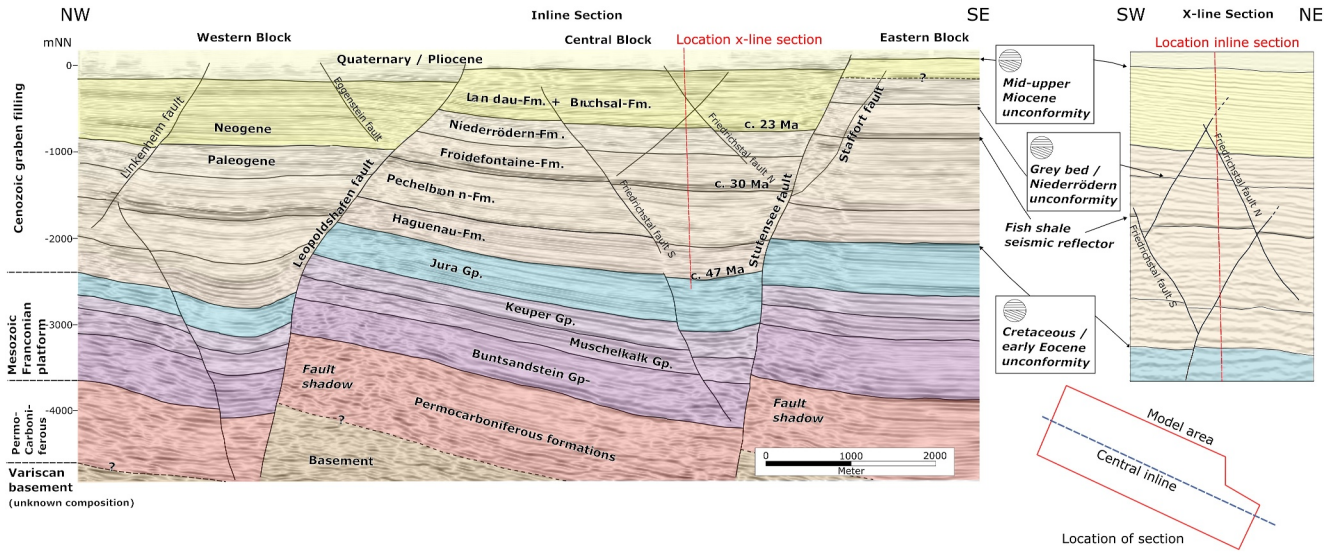

Figure 4. Inline and cross-line sections from the central part of the survey showing the stratigraphy, major unconformities, and thickness distributions in the three (Western, Central, Eastern) tectonic blocks separated by the deep rooted Leopoldshafen and Stutensee faults, regarded to displace the crystalline basement. Presence and thickness of Permocarboniferous is presumed from regional trends (Geyer et al., 2011), not constrained by wells.

as seismic marker horizons (i.e., Top Lymnaea Marls, Top Middle Pechelbronn beds, and Top Upper Pechelbronn beds). However, differentiation into Lower, Middle and Upper Pechelbronn beds requires supporting borehole information. The overlying Froidefontaine Fm. (Gray Bed Series) is seismically subdivided into the marker horizons of Top Fish Shale, Top Meletta beds, and Top Cyrena Marls. In the URG, the combined Fish Shale and Foraminifera Marl ("Rupel Clay") form a basin-wide seismic marker horizon with high amplitudes and low to medium frequencies, which can be traced as a parallel reflector bundle. This reflector bundle, tied to four boreholes, served as a reliable starting point for structural-stratigraphic mapping in the study area. The Rupel Clay is also characterized by a distinct decrease of seismic velocities and an increase of gamma ray activities. The reflectors of the Meletta beds and Cyrena Marls have low amplitude and continuity, making seismic delineation challenging, but borehole and log data enable further differentiation (Figure 2).

The seismic marker horizons of the Top Niederrödern Formation, Top Cerithia beds, and Top Corbicula beds are well defined by high-amplitude reflectors. The marls and sandstones of the Niederrödern Formation are imaged as a group of well-defined reflectors. Reflectors in the Niederrödern Fm., particularly at the top, show an impedance contrast compared to the Cerithia beds in the hanging wall, with the Corbicula beds displaying larger seismic amplitudes. The base of the Niederrödern Fm. marks another unconformity, well displayed in the cross-line sections, but less well in the inline sections (Figures 3 and 4).

Recent stratigraphy combines the Cerithia and Corbicula beds into the Bruchsal Formation (Geyer et al., 2011). The Landau Formation (Lower and Upper Hydrobia beds) is unconformably overlain by the base of the Pliocene, which, combined with Quaternary successions, forms the uppermost unit.

3.2. Major Structures

The deep rooted Leopoldshafen and Stutensee faults strike NNE and subdivide the study area into a Western, Central, and Eastern block which comprise a group of SE-tilted blocks (Figure 4). The shallow rooted Linkenheim and Eggenstein faults as well as the en-echelon Friedrichstal faults structure the respective hanging walls of the Leopoldshafen and Stutensee faults and control geometry of N(NW)-trending structural basins and swells in the Western and Central blocks. The W-dipping Leopoldshafen and the WNW-dipping Stutensee faults exhibit throws of up to about 900 and 600 m, respectively, in the study area (Figure 4). Both faults most likely intersect the crystalline basement and are therefore regarded as deep-rooted crustal faults (Figure 4). In the Cenozoic successions, the Leopoldshafen and Stutensee faults dip about 50° to the W and about 60–70° to the WNW, respectively, steepening to about 80° in the Mesozoic successions. Distinct, ≥400 m thick Neogene syntectonic sediments in the hanging wall of the Leopoldshafen fault document growth faulting (Figure 4). Neogene growth

10.1029/2024TC008721

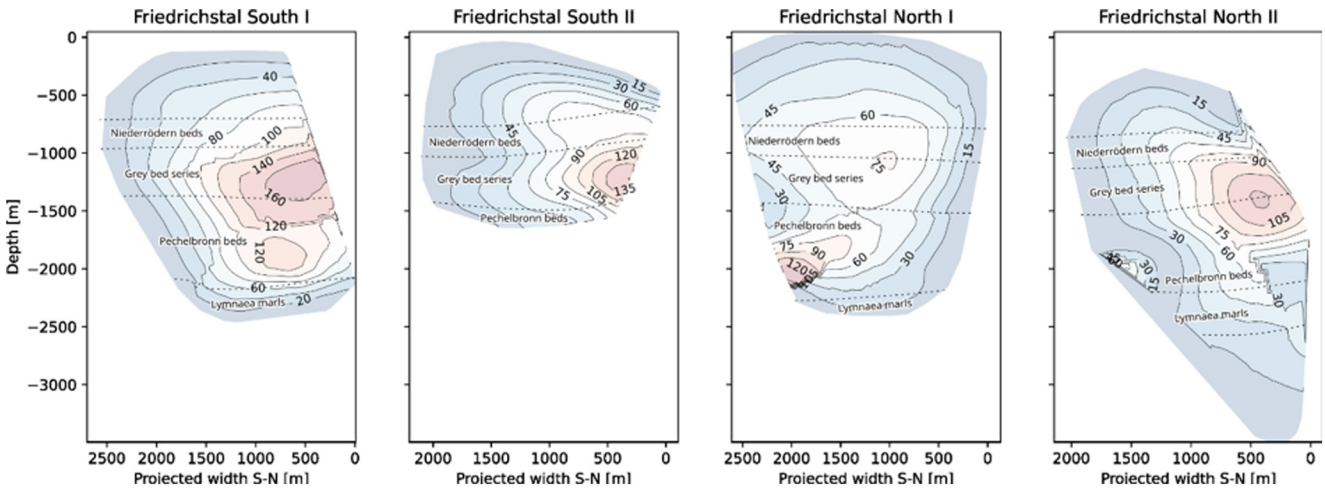

Figure 5. Fault nucleation diagrams of the four projected individual Friedrichstal fault segments with isolines and color ramps of displacement in meters.

faulting generated the syncline of the hanging wall in Eocene-Oligocene strata to compensate downdip extension (Figure 4). Quaternary faulting is indicated by 7–14 m displacement of Quaternary-Pliocene successions (Bartz, 1982). Latest Oligocene and Neogene growth strata in the hanging wall of the Stutensee fault suggest Neogene to Pleistocene normal faulting activity, but the distribution of late Oligocene-Neogene successions appear to be controlled by the NNW-striking Friedrichstal faults in the hanging wall of the Stutensee fault, as discussed below.

In the Pechelbronn Fm., the Staffort fault developed in the footwall of the Stutensee fault as a shallow rooted fault (Figure 4). The largest displacements are accommodated by the Stutensee fault. Toward N, a N-plunging relay ramp developed between the Staffort and the Stutensee faults. The N-S striking Linkenheim fault dipping about 60° to the west, outlines max. displacements of about 150 m and a strike length of about 2.5 km. The Linkenheim fault displaced Cenozoic sequences only and is therefore regarded as a shallow rooted fault as well (Figure 4). The four segments of the Friedrichstal faults are 2–2.5 km long showing displacements between 75 and 160 m (Figure 5). They terminate in Cenozoic strata and are therefore shallow rooted faults as well (Figures 4 and 5).

The Friedrichstal faults nucleated mainly in the Gray Bed Series (Figure 5), where they formed first as normal fault segments of two small NNW-trending graben structures with convergent, opposed-dipping normal segments, which intersect each other in the Pechelbronn beds (Figure 6). Stratigraphically upwards, the two inner faults intersect each other in the Corbicula beds and develop as divergent opposed-dipping faults in the Hydrobia beds, where the Friedrichstal faults, except for the easternmost, E-dipping fault segment, were apparently sealed, that is, within the resolution of 3D-seismic imaging (Figures 5 and 6). The displacements of the W-dipping faults die out toward south and hence were not cut by the Stutensee fault (Figures 4 and 6), forming a composite conjugate relay ramp system (Figures 4 and 6–8).

3.3. Sedimentary Thickness Distributions

The slightly SE-dipping, early Cenozoic successions overlie unconformably slightly steeper dipping sequences from the Middle Jurassic (Figure 4). Pre-rift Cenozoic successions such as the Eocene Schliengen Fm. are reported with thicknesses of 12 and 15 m from in-field boreholes and few off-site boreholes in the northeast of the study area. These thicknesses are below resolution of seismic data and therefore the Schliengen Fm. could not be mapped as a discrete unit.

Thicknesses of the overlying successions in the three blocks vary as well as strike and dip of bedding (Figure 6). The middle to late Eocene Lymnaea marls (Haguenau Fm.) comprise the earliest, spatially extensively deposited syn-rift sequences. They occur at depths below approximately 2,400 m and 1,600 m below sea level in the Western and Eastern blocks, respectively, with thicknesses increasing from the Eastern to the Western block (Figure 6e). In the Eastern block, isopachs and violin plots show a relatively homogeneous thickness distribution varying between 330 and 390 m, slightly increasing toward E (Figure 6e). In the Central block, larger thicknesses

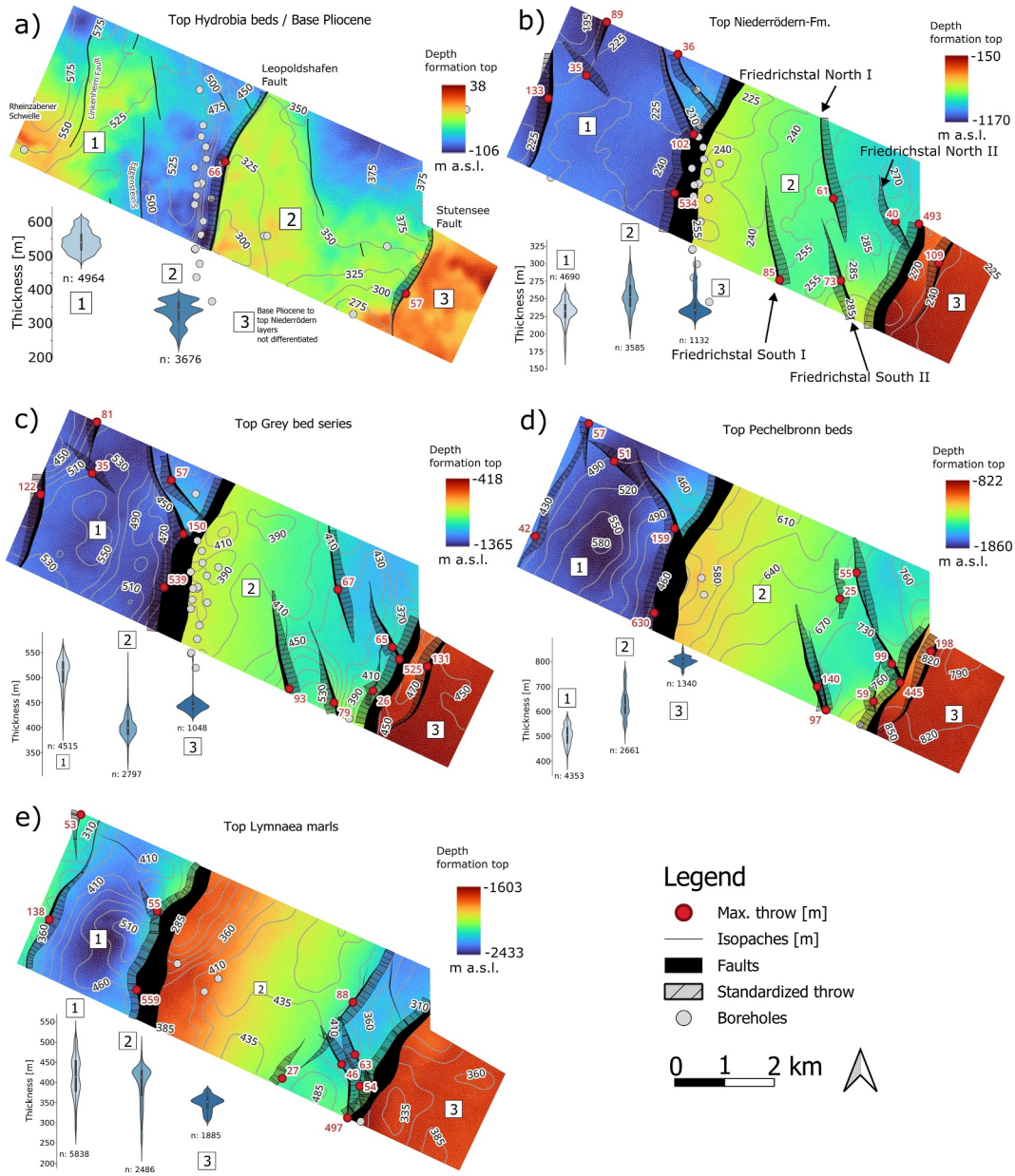

Figure 6. (a–e) Color coded depth distribution map of selected formation tops as indicated by the headers. Color coded depth range in meter above sea level (m a.s.l.) is shown in the legend of individual formation top map. Isopach contour lines of the Gray Bed series are labeled with thicknesses (in m). Black polygons mark projected faults. Attached to the fault traces are the normalized displacements on the hanging wall of the respective normal faults. Red circles mark the location and red numbers the amount of maximum displacement (in m) along individual faults. Faults with displacements <20 m were neglected. Light-gray circles mark intersections of formation top with boreholes. Thickness distributions are displayed as violin plots from point data from the respective (1) Western, (2) Central, (3) Eastern block.

are more variable, but generally increasing toward SE. Between the antithetic fault E of the Stutensee fault and the latter, thicknesses decrease significantly toward N. The thicknesses in the hanging wall of the Leopoldshafen fault vary between 250 and 550 m. The increase in thickness is related to the large displacements on the two major faults: In the hanging wall of these faults are synformal half-graben basins that are bounded to the W by antithetic faults. These antithetic faults can be traced in the 3D seismic imaging down into the Mesozoic strata showing throws about 140 m (Leopoldshafen fault) and about 90 m (Stutensee fault) of Top Haguenau Fm., which form early syn-rift basins during (W)NW extension. The synformal geometry may result from convergence due to

10.1029/2024TC008721

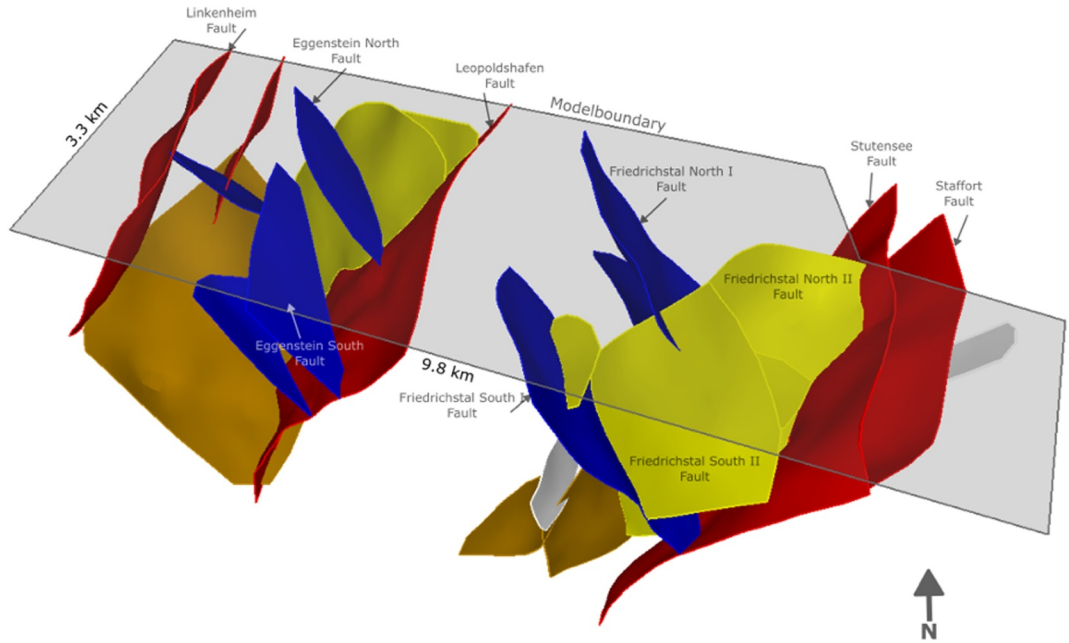

Figure 7. 3D geometry of modeled faults in the survey area.

steepening of the fault with depth (Figure 4). The thicknesses, dip directions and angles of the bedding vary within the western and eastern areas of the Central block, resulting in a prism-shaped basin fill corresponding to the syn-rift deposition and rotation along a subhorizontal axis of the hanging wall of the Stutensee fault. The Central block is also characterized by SE dipping strata with increasing dip angles toward the Leopoldshafen fault. The angular unconformity between Jurassic and Cenozoic strata variable dip angles from 4° to 2.5° in the Eastern block, from 12° to 6.5° in the Central block, while in the Western block both, Jurassic and basal Cenozoic strata, dip c. 15°. This angle decreases toward the upper part of the Lymnaea marls, which indicates a successive filling in the hanging wall of the Leopoldshafen fault.

The thickness of the Pechelbronn Fm. varies between 450 and 850 m (Figure 6d). In contrast to the Lymnaea marls, it increases toward east, possibly related with major normal displacement along the Eastern Main Boundary fault of the URG, outside the study area. Thickness variations in the Pechelbronn Fm. indicate growth faulting and filling up of early Cenozoic depocenters developed during deposition of the Lymnaea marls. Possibly due to the antithetic faulting, the local depositional center in the hanging wall of the Leopoldshafen fault has expanded with time. Lower thicknesses of about 400–600 m in the Western block compared to up to 850 m in the Eastern block indicate a comparably low activity of this fault. During deposition of the Pechelbronn Fm. the minor antithetic fault of the Stutensee fault was buried, which also indicates faulting activity along the Eastern Main Boundary fault. In the Central block, the dip direction changes slightly to the N and decreases in dip. In the upper part of the Pechelbronn Fm., the shallow rooted, W-dipping Linkenheim fault can be mapped. The Stutensee fault is split into two fault segments with the more easterly Staffort fault segment dying out toward SE.

The Fish shale outlines relatively low thicknesses of 10–20 m in the Central block. These thinly sheeted clays and marls are overlain by the Meletta beds and Cyrena marls. In these latter two units, several meter-thick sandstone layers are identified from the SP- and RES-logs. While the thickness of the Gray Bed series increases toward the west, the synform in the hanging wall of the Leopoldshafen fault expanded, but sedimentary thicknesses, varying less than 40 m, do not indicate a major depocenter formation associated with this synform (Figure 6c). At the western limit of this block, in the Linkenheim fault, a soft-linked relay ramp structure develops causing a local structural swell leading to a reduced thickness of about 400 m. Along the two en-echelon Eggenstein faults, displacements of about 150 m are observed. The thickness distributions in the individual blocks, with maxima in the E and W, indicate larger displacements along the Leopoldshafen fault and, second, the Eastern Main Boundary fault. A reduced displacement rate along the Stutensee fault resulted in a change in morphology on the top of the Gray Bed series with a change in dip directions to the E and a dip angle of about 7° in the western part of the

10.1029/2024TC008721

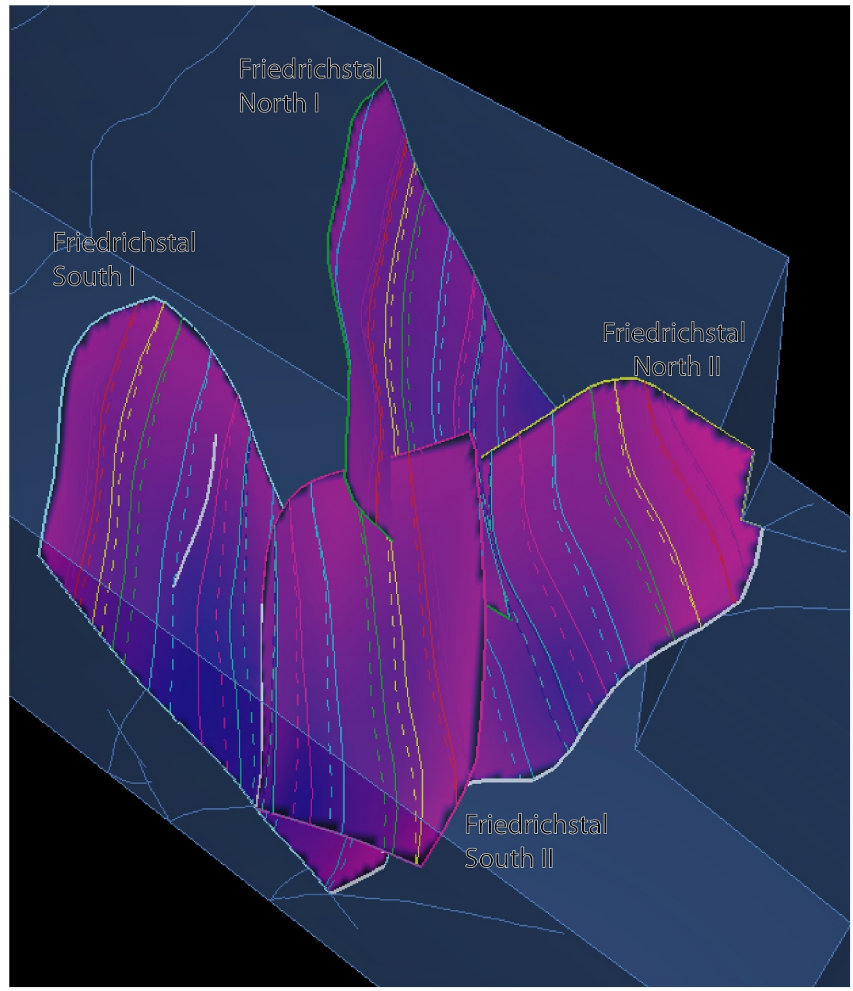

Figure 8. Isolated Friedrichstal faults, displaying a complex conjugate relay ramp system. Stippled lines mark intersection of seismic marker horizons in the hanging wall of modeled fault surface, continuous lines mark intersection of seismic marker horizons in the footwall of modeled fault surface.

Central block. The synform in the hanging wall of the Stutensee fault were filled and offset by the N-trending en-echelon Friedrichstal fault segments, which developed soft-linked relay ramps between the different segments. The Linkenheim, Eggenstein, and Friedrichstal faults show their maximum displacements in the Gray Bed series (Figure 5), indicating nucleation within these sequences, whereas the main normal faults nucleated in older strata.

Compared to the Gray Bed series, the thickness difference between the blocks is less pronounced in the Niederrödern Formation, indicating generally low(er) tectonic activity (Figure 6b). The sandstone layers of the Niederrödern Formation reach thicknesses >10 m. Although the dip angles of the reflectors are comparatively smaller, that is, less than 2° based on borehole data correlation, an unconformity can be variably well mapped in the cross-line sections, but less in the inline sections. Also, within the Central block this unconformity can be better documented than in the Western and Eastern blocks. West of the Leopoldshafen fault, isopachs do not indicate a depositional center, but the basin east of the Friedrichstal faults expands by continuous displacement along the fault set dipping in the opposite direction. Small differences in thickness variation between the three blocks and the nucleation of the Friedrichstal faults in the Gray Bed series suggest strain migration from the deep rooted faults to initiate the shallow rooted en-echelon faults.

To analyze the youngest phase of the basin development, Cerithia, Corbicula, and Hydrobia beds (Bruchsal- and Landau-Formations) are combined in the following discussion. Although data density and quality are low in the Eastern block, the unconformity between the Pliocene and Miocene successions is mapped and verified based on

analysis of stratigraphic data from deep groundwater wells (Bartz, 1982). A maximum thickness of the Hydrobia beds of up to 550 m is observed in the Western block (Figure 6e), whereas in the Central block, the maximum thickness is about 350 m. This is attributed to significant displacements along the Leopoldshafen and, to a lesser extent, the Stutensee faults. In the hanging wall of the Leopoldshafen fault, the N-S trending Neogene depocenter formed between the Leopoldshafen and the southern Eggenstein faults. A similar scenario is observed in the northeastern part of the Central block: Comparably smaller displacement along the Stutensee fault leads to moderate thickness but larger strike and dip changes. The en-echelon faults disappear, but the remaining active parts of the faults were shifted to the center of the block. At the western edge of our model, Hydrobia beds occur about 30 m above sea level (or c. 70–80 m below the surface), constituting the eastern part of the "Rheinzabern swell," which is one of few Neogene structural highs W of the Rhine river (e.g., Bartz, 1982).

4. Discussion

4.1. Structural Development and Stress Field Change

Stress interactions within and between adjacent fault systems may control the nucleation, migration and death of faults during progressive deformation (Cowie et al., 2005). The nucleation of the shallow rooted faults in the Central block was accompanied by a reduction of throw of the Stutensee fault in the respective Oligocene strata. This indicates a kinematic coupling between these faults and raises the question why new faults initiated instead of persisting activity. We cannot rule out that the reduction of throw at the Stutensee fault was compensated by a lateral component of fault displacement as commonly only the amount of throw can be well imaged in 3D-seismic surveys, unless well-defined markers exist indicating lateral displacements. At least for the shallow rooted faults projection of displacements on fault planes suggests an origin as elliptical normal faults (Figure 5) and thus there is no major reason to assume lateral movements along individual fault segments. In addition, the composite conjugate relay ramp system, documented first in the URG (Figures 6–8), implies that lateral displacements can be neglected for the Friedrichstal faults. Formation processes of shallow rooted faults may encompass (a) soft-linked reactivation of deeper structures, (b) low-friction slip plane (re-)activation, gravitational forces, and (c) regional stress field changes (e.g., Samsu et al., 2023; Wrona et al., 2017).

The formation of newly formed shallow rooted faults, deviating in strike directions from the deep rooted faults by angles of 35–45°, mark a change of the deformation style and orientation of the overall extension direction during rift development, which was most likely a response to a change of the external, regional stress field orientation. As nucleation of these shallow rooted faults occurred within 32 Ma to 28 Ma old strata (Figure 5), we propose a change of the regional stress field and associated changes of the strain axes that could not cause development of these new faults earlier than 32 Ma. The Leopoldshafen and Stutensee faults display syn-rift 2 growth faulting with larger thicknesses in their hanging wall blocks implying major normal displacement concomitantly active with the shallow rooted faults. Major lateral displacements along the deep rooted faults are thus rather unlikely and hence also a soft linked reactivation of the shallow rooted faults. We thus think that the initiation of the shallow rooted faults is caused by a change of the regional stress field. While for the shallow rooted faults orientation of principal stress axes is expected to be parallel and normal, respectively, to the earth's surface, at greater depths orientations of principal stress axes may be oblique relative to earth's surface. The latter may be influenced by preexisting major faults (e.g., Homberg et al., 1997) or a general obliquity of external dynamic forces. We therefore propose that the regional stress field changed from general (W)NW- to general (E)NE-extension during late Oligocene times, that is, at c. 27 ± 1 Ma.

4.2. Superposition of Intra-Rift Basins

The change of deformation style and development of shallow rooted faults generated new intra-rift basins trending N-S to NNW-SSE superposing older (N)NE-trending rift basins with an unconformity at the base of the Niederrödern Fm., which is well imaged in some areas of the survey. Therefore, we subdivide the stratigraphy into syn-rift 1 and syn-rift 2 (Figure 2). Thickness distributions of syn-rift 1 successions indicate growth faulting during general NW- to WNW-extension (Figures 4 and 6). Sedimentation in rifts is mainly controlled by episodic faulting followed by periods of relative tectonic quiescence expressed by progradation filling up accommodation space (e.g., Martins-Neto & Catuneanu, 2010). Syn-rift 2 phase started with unconformable deposition of the predominantly fluvio-lacustrine sediments of the Niederrödern Fm. on the partly exposed Cyrena marls. The latter

10.1029/2024TC008721

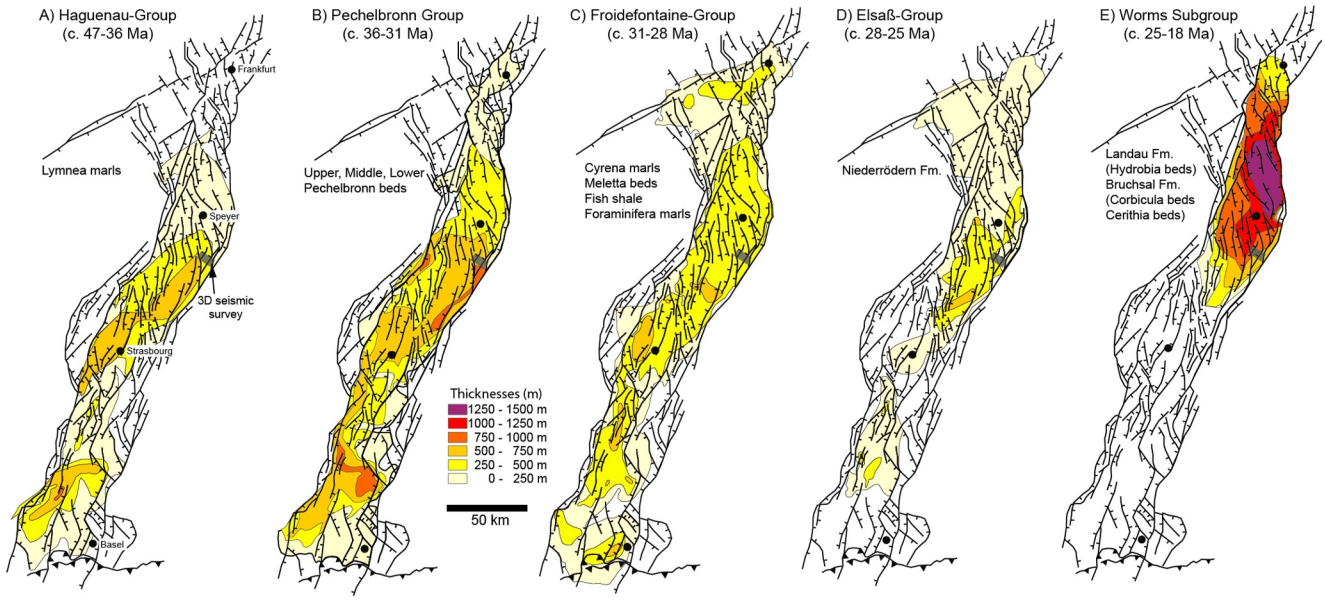

Figure 9. Development of basin filling with time at the rift basin scale indicating a shift from syn-rift 1 depocenters in the southern and central segment to the major syn-rift 2 depocenter of the Heidelberg basin during latest Oligocene to early Miocene times (modified from Grimm et al. (2011) and Grimmer et al. (2017)).

unit includes the regressive system tract, deposited on the transgressive system tract of the middle to upper Meletta beds (Pirkenseer et al., 2013). The regressive Cyrena marls mark onset of the Chattian regression phase and the unconformable deposition of the Niederrödern Fm. A relationship between stress field change and Chattian regression seems to be likely, but further detailed work is needed to resolve structural-stratigraphic development during this time period. Concomitantly with syn-rift 2 minor alkaline silica undersaturated volcanic rocks intruded and extruded in the URG and surrounding areas (Binder et al., 2023) as for example, N-S-striking olivine melilitite dykes exposed in a former potash salt mine, dated to 25 ± 2 Ma, intrusive into deformed Oligocene strata in the southern URG, indicating local E-W extension, and the Miocene Kaiserstuhl volcanic edifice, dated to 18–14 Ma (Binder et al., 2023). Thickness variations in the fluvio-lacustrine Niederrödern Fm. are ≤50 m (Figure 6b), indicating the filling of accommodation space and a relative tectonic quiescence (Figure 6b). Concomitantly with the nucleation of the Friedrichstal faults in the Froidefontaine Fm. a change in structural basin trends from (N)NE to N(NW) is observed and thickness variations became less. This structural trend progressively developed during early Miocene times. Thus, we propose that the rift-external, regional stress field changed from (W)NW-extension to NE-extension during onset of deposition of the c. 28–25 Ma Niederrödern Fm. and onset of a new type of intra-rift basins, which differ from syn-rift 1 half-graben basins as they formed on top of them in the hanging wall of major deep rooted faults, but were internally structured by newly formed en-echelon shallow rooted faults. However, rift internal stress and strain axes may slightly deviate from external stress and strain axes due to progressive transtensional deformation and other factors influencing stress axes orientations and magnitudes (e.g., rheological contrasts, pre-existing faults) generating N-S to NNW-SSE trending intra-rift basins. We propose that this basin formation style is not limited to our small seismic survey but is more widespread in the URG as this basin trend is also reflected in the N-trending intra-rift Heidelberg basin (Figures 1 and 9).

In the hanging wall of the Leopoldshafen fault, early Miocene reactivation created a synform along the hinge line of the steepening fault. In contrast, the antithetic fault associated with the Stutensee fault displaced the lowermost Cenozoic rocks but, unlike the antithetic fault of the Leopoldshafen fault, did not displace the Pechelbronn Fm. These antithetic normal faults were buried by late Eocene and early Oligocene strata (Figure 6b). WNW-dipping formation tops of Eocene-early Oligocene strata also indicate rotation around NNE-axes resulting from WNW extension. The N- to NNW-trend in the Niederrödern Fm., which is controlled by the shallow rooted, en-echelon Friedrichstal and Eggenstein faults (Figure 6b), indicates that this style of deformation changes during the

transition from syn-rift phase 1 to 2. The nucleation of the Friedrichstal, Eggenstein, and Linkenheim faults occurred between 32 Ma and 28 Ma old strata (Figure 5). During latest Oligocene times, the major depocenter of the URG has shifted to the northern segment of the URG forming the distinct N-trending Heidelberg basin (Figure 9). In our study area this is supported by the observed counter-clockwise rotation of the strike direction from NNE to N of the Niederrödern Fm. and the subsequently younger successions that indicate the onset of N-S-trending basins during late Oligocene times. The Friedrichstal, Eggenstein, and Linkenheim faults started to control distribution and accumulation of late Oligocene and early Miocene successions and hence basin development in the respective hanging wall of the major deep rooted faults that need to be reactivated as (oblique?) normal faults (Figure 6). This also corroborates our sub-division of the stratigraphic succession into syn-rift 1 (between c. 47–27 Ma) and syn-rift 2 (from c. 27 ± 1 Ma to at least 16 Ma and possibly until today, Figure 2).

While the syn-rift 1 phase is characterized by an essentially continuous sedimentary record, the syn-rift 2 phase was interrupted by a phase of mid-/late Miocene uplift and erosion, possibly due to a phase of dynamic topography affecting predominantly the southern to central segments of the URG for more than 10 Myr (Binder et al., 2023). This time period coincides with the Late Oligocene to Miocene South Central European Volcanic Province (S-CEVP) starting to produce volcanic rocks in NE-France and SW-Germany at c. 25–26 Ma (Binder et al., 2023), attributed to the reactivation of deep rooted faults within this newly established stress field. Since the Late Oligocene—Early Miocene stress field shows an ENE orientation of the minimum horizontal stress (S_{hmin}) that is similar the present orientation, we may hypothesize that it persists since c. 27 ± 1 Myr. Consequently, the mid to late Miocene uplift superposed the regional stress and deformation field without significant modification of the stress axes orientations but did affect the stress magnitudes. While the shallow rooted Friedrichstal, Linkenheim, and Eggenstein faults represent structures that formed during syn-rift 2, the deep rooted Leopoldshafen and Stutensee faults were reactivated as (oblique?) normal faults. The N- to NNW-trending Neogene syn-rift 2 basins superpose earlier NNE-trending syn-rift 1 basins and are thus controlled geometrically by these newly formed shallow rooted and reactivated deep rooted (oblique?) normal faults (Figure 6).

We have yet little quantitative data to characterize rates and processes of this regional stress field change in the URG. We speculate that stress field change was related with completion of mechanical coupling of the lower European plate with the overriding Alpine orogenic wedge and the Upper Adriatic plate, possibly related to slab-breakoff, and a change from marine underfilled to continental overfilled basin development at least in the western Molasse basin (e.g., Kempf & Pross, 2005; Sinclair, 1997). Time transgressive unconformable deposition of the Lower Freshwater Molasse, started earliest at c. 30 Ma and was widespread in the western Molasse basin at c. 28 Ma indicating the transition from underfilled to overfilled basin in the western Molasse basin (e.g., Kempf & Pross, 2005; Ortner et al., 2015; Schlunegger et al., 1997). In summary, we propose that regional stress field change did not initiate before 30 ± 2 Ma and was established during deposition of the Niederrödern Fm. at 27 ± 1 Ma.

5. Conclusions

Intra-rift basin development in the northern part of the central segment of the URG is controlled by a change of the regional stress field established at 27 ± 1 Ma, that is, during unconformable deposition of the Niederrödern Fm. Thus, stratigraphy is subdivided into syn-rift 1 and syn-rift 2 successions. Syn-rift 1 basin axes trend NE to NNE, syn-rift 2 basin axes trend N and are controlled by shallow rooted en-echelon faults that nucleated within 32–28 Ma old strata. These newly formed shallow rooted en-echelon faults constitute a set of conjugated relay ramps. Syn-rift 2 basins superposed syn-rift 1 basins by reactivating deep rooted faults as (oblique?) normal faults initiating the recent style of deformation and basin formation as reflected by the distinct Heidelberg basin. We suggest that stress field change was induced by mechanical coupling between the lower European plate and the overriding Adriatic upper plate possibly associated with slab break-off.

Data Availability Statement

For the structural modeling we used the software Petrel of SLB (academic license). The 3D seismic data were purchased and reprocessed by the authors for scientific assessment from the industrial data owners. Due to the German Geodata act 3D seismic data may be provided by Federal Authorities if the necessary legal requirements are fulfilled to purchase the data.

Acknowledgments
Funding of this study, which is part of the subtopic "Geoenergy" in the program "Materials and Technologies for the Energy Transition (MTET)," by the Helmholtz Association, discussions with Thomas Kohl and Dominik Gudelius during different stages of work progress, and support of our work by Neptune Energy GmbH and their consortial partners as well as constructive comments of Associate editor Laura Giambiagi, William Bosworth, and an anonymous reviewer improved the manuscript and are gratefully acknowledged. The modeling work was conducted using the Petrel software by Schlumberger, whose support is gratefully acknowledged. Open Access funding enabled and organized by Projekt DEAL.

References

Acocella, V., Morvillo, P., & Funiciello, R. (2005). What controls relay ramps and transfer faults within rift zones? Insights from analogue models. *Journal of Structural Geology*, *27*(3), 397–408. https://doi.org/10.1016/j.jsg.2004.11.006

Agostini, A., Corti, G., Zeoli, A., & Mulugeta, G. (2009). Evolution, pattern, and partitioning of deformation during oblique continental rifting: Inferences from lithospheric-scale centrifuge models. *Geochemistry, Geophysics, Geosystems*, *10*(11), Q11015. https://doi.org/10.1029/2009GC002676

Bartz, J. (1982). Quartär und Jungtertiär II im Oberrheingraben im Großraum Karlsruhe. *Geologisches Jahrbuch A*, *63*, 3–237.

Berger, J.-P., Reichenbacher, B., Becker, D., Grimm, M., Grimm, K., Picot, L., et al. (2005). Eocene-Pliocene time scale and stratigraphy of the Upper Rhine Graben (URG) and the Swiss Molasse Basin (SMB). *International Journal of Earth Sciences*, *94*(4), 711–731. https://doi.org/10.1007/s00531-005-0479-y

Binder, T., Marks, M. A. W., Gerdes, A., Walter, B. F., Grimmer, J., Beranoaguirre, A., et al. (2023). Two distinct age groups of melilitites, foidites, and basanites from the southern Central European Volcanic Province reflect lithospheric heterogeneity. *International Journal of Earth Sciences*, *112*(3), 881–905. https://doi.org/10.1007/s00531-022-02278-y

Böcker, J., Littke, R., & Forster, A. (2017). An overview on source rocks and the petroleum system of the central Upper Rhine Graben. *International Journal of Earth Sciences*, *106*(2), 707–742. https://doi.org/10.1007/s00531-016-1330-3

Bosworth, W., Huchon, P., & McClay, K. (2005). The Red Sea and Gulf of Aden basins. *Journal of African Earth Sciences*, *43*(1–3), 334–378. https://doi.org/10.1016/j.jafrearsci.2005.07.020

Brune, S. (2014). Evolution of stress and fault patterns in oblique rift systems: 3-D numerical lithospheric-scale experiments from rift to breakup. *Geochemistry, Geophysics, Geosystems*, *15*(8), 3392–3415. https://doi.org/10.1002/2014gc005446

Brune, S., Corti, G., & Ranalli, G. (2017). Controls of inherited lithospheric heterogeneity on rift linkage: Numerical and analog models of interaction between the Kenyan and Ethiopian rifts across the Turkana depression. *Tectonics*, *36*(9), 1767–1786. https://doi.org/10.1002/2017TC004739

Corti, G., van Wijk, J., Cloetingh, S., & Morley, C. K. (2007). Tectonic inheritance and continental rift architecture: Numerical and analogue models of the East African Rift system. *Tectonics*, *26*(6), TC6006. https://doi.org/10.1029/2006TC002086

Cowie, P. A., Underhill, J. R., Behn, M. D., Lin, J., & Gill, C. (2005). Spatio-temporal evolution of strain accumulation derived from multi-scale observations of Late Jurassic rifting in the northern North Sea: A critical evaluation of models of lithospheric extension. *Earth and Planetary Science Letters*, *234*(3–4), 401–419. https://doi.org/10.1016/j.epsl.2005.01.039

Derer, C. E., Schumacher, M. E., & Schäfer, A. (2005). The northern Upper Rhine Graben: Basin geometry and early syn-rift tectono-sedimentary evolution. *International Journal of Earth Sciences*, *94*(4), 640–656. https://doi.org/10.1007/s00531-005-0515-y

Esslinger, G. (1976). Vorkommen und Tektonik der Basalte im Kalisalzlager Buggingen. *Jahreshefte geologisches Landesamt Baden-Württemberg*, *18*, 7–18.

Eynatten, H., Kley, J., Dunkl, I., Hoffmann, V.-E., & Simon, A. (2021). Late Cretaceous to Paleogene exhumation in central Europe – Localized inversion vs. large-scale domal uplift. *Solid Earth*, *12*(4), 935–958. https://doi.org/10.5194/se-12-935-2021

Fuhrmann, T., Cuenca, M. C., Knöpfler, A., van Leijen, F. J., Mayer, M., Westerhaus, M., et al. (2015). Estimation of small surface displacements in the Upper Rhine Graben area from a combined analysis of PS-InSAR, levelling and GNSS data. *Geophysical Journal International*, *203*(1), 614–631. https://doi.org/10.1093/gji/ggv328

Gabriel, G., Ellwanger, D., Hoselmann, C., Weidenfeller, M., & Wielandt-Schuster, U. (2013). The Heidelberg Basin, Upper Rhine Graben (Germany): A unique archive of Quaternary sediments in Central Europe. *Quaternary International*, *292*, 43–58. https://doi.org/10.1016/j.quaint.2012.10.044

GeORG-Projektteam. (2013). Geopotentiale des tieferen Untergrundes im Oberrheingraben, *Fachlich-Technischer Abschlussbericht des Interreg-Projekts GeORG. Teile 1-4*.

Geyer, M., Nitsch, E., & Simon, T. (2011). Geologie von Baden-Württemberg (5th ed., p. 627).

Golombek, M. P., McGill, G. E., & Brown, L. (1983). Tectonic and geologic evolution of the Española Basin, Rio Grande Rift: Structure, rate of extension, and relation to the state of stress in the western United States. *Tectonophysics*, *94*(1–4), 483–507. https://doi.org/10.1016/0040-1951(83)90031-8

Grimm, M., Wielandt-Schuster, U., Hottenrott, M., Grimm, K. I., & Radtke, G. (2011). Oberrheingraben. In Deutsche Stratigraphische Kommission (Ed.), *Stratigraphie von Deutschland IX. Tertiär, Teil 1*, *Schriftenreihe der Deutschen Gesellschaft für Geowissenschaften* (Vol. 75, pp. 57–131).

Grimmer, J. C., Ritter, J. R. R., Eisbacher, G. H., & Fielitz, W. (2017). The Late Variscan control on the location and asymmetry of the Upper Rhine Graben. *International Journal of Earth Sciences*, *106*(3), 827–853. https://doi.org/10.1007/s00531-016-1336-x

Homberg, C., Hu, J. C., Angelier, J., Bergerat, F., & Lacombe, O. (1997). Characterization of stress perturbations near major fault zones: Insights from 2-D distinct-element numerical modelling and field studies (Jura mountains). *Journal of Structural Geology*, *19*(5), 703–718. https://doi.org/10.1016/s0191-8141(96)00104-6

Kallweit, R. S., & Wood, L. C. (1982). The limits of resolution of zero-phase wavelets. *Geophysics*, *47*(7), 1035–1046. https://doi.org/10.1190/1.1441367

Kärcher, T. (1987). Beiträge zur Lithologie und Hydrogeologie der Lockergesteinsablagerungen (Pliozän, Quartär) im Raum Frankenthal, Ludwigshafen, Mannheim, Speyer. *Jahresberichte und Mitteilungen des Oberrheinischen Geologischen Vereins*, *69*, 279–320. https://doi.org/10.1127/jmogv/69/1987/279

Kempf, O., & Pross, J. (2005). The lower marine to lower freshwater Molasse transition in the northern Alpine foreland basin (Oligocene; central Switzerland–south Germany): Age and geodynamic implications. *International Journal of Earth Sciences*, *94*(1), 160–171. https://doi.org/10.1007/s00531-004-0437-0

Lutz, M., & Cleintuar, M. (1991). Geological results of a hydrocarbon exploration campaign in the southern Upper Rhine Graben (Alsace Centrale, France). *Bulletin für Angewandte Geologie*, *4*, 3–80.

Mälzer, H. (1988). Regional and local kinematics in SW-Germany by geodetic methods—Geophysical and geological interpretation. *Journal of Geodynamics*, *9*(2), 141–151. https://doi.org/10.1016/s0264-3707(88)80057-7

Martins-Neto, M. A., & Catuneanu, O. (2010). Rift sequence stratigraphy. *Marine and Petroleum Geology*, *27*(1), 247–253. https://doi.org/10.1016/j.marpetgeo.2009.08.001

NASA JPL. (2013). NASA Shuttle Radar Topography Mission Global 1 arc second [Dataset]. *NASA EOSDIS Land Processes Distributed Active Archive Center*. https://doi.org/10.5067/MEaSUREs/SRTM/SRTMGL1.003

Ortner, H., Aichholzer, S., Zerlauth, M., Pilser, R., & Fügenschuh, B. (2015). Geometry, amount, and sequence of thrusting in the Subalpine Molasse of western Austria and southern Germany, European Alps. *Tectonics*, *34*(1), 1–30. https://doi.org/10.1002/2014TC003550

Pirkenseer, C., Berger, J.-P., & Reichenbacher, B. (2013). The position of the Rupelian/Chattian boundary in the southern Upper Rhine Graben based on new records of microfossils. *Swiss Journal of Geosciences*, *106*(2), 291–301. https://doi.org/10.1007/s00015-013-0146-4

Randen, T., Monsen, E., Signer, C., Abrahamsen, A., Schlaf, J., Sæter, T., & Hansen, J. O. (2000). Three-dimensional texture attributes for seismic data analysis. In *SEG International Exposition and Annual Meeting*. SEG-2000-0668.

Reinhold, C., Schwarz, M., Bruss, D., Heesbeen, B., Perner, M., & Suana, M. (2016). The Northern Upper Rhine Graben: Re-dawn of a mature petroleum province. *Swiss Bulletin*, *21*, 35–56.

Ring, U. (1994). The influence of preexisting structure on the evolution of the Cenozoic Malawi rift (East African rift system). *Tectonics*, *13*(2), 313–326. https://doi.org/10.1029/93TC03188

Rotstein, Y., Behrmann, J. H., Lutz, M., Wirsing, G., & Luz, A. (2005). Tectonic implications of transpression and transtension: Upper Rhine Graben. *Tectonics*, *24*(6), TC6001. https://doi.org/10.1029/2005TC001797

Samsu, A., Micklethwaite, S., Williams, J. N., Fagereng, Å., & Cruden, A. R. (2023). Structural inheritance in amagmatic rift basins: Manifestations and mechanisms for how pre-existing structures influence rift-related faults. *Earth-Science Reviews*, *246*, 104568. https://doi.org/10.1016/j.earscirev.2023.104568

Schad, A. (1964). Feingliederung des Miozäns und die Deutung der nacholigozänen Bewegungen im Mittleren Rheingraben: Eine Auswertung erdölgeologischer Arbeiten. *Abhandlungen des Geologischen Landesamtes Baden-Württemberg*, *5*, 1–56.

Schlunegger, F., Matter, A., Burbank, D. W., Leu, W., Mange, M., & Màtyàs, J. (1997). Sedimentary sequences, seismofacies and evolution of depositional systems of the Oligo/Miocene Lower Freshwater Molasse Group, Switzerland. *Basin Research*, *9*, 1–26. https://doi.org/10.1046/j.1365-2117.1997.00029.x

Schumacher, M. E. (2002). Upper Rhine Graben: Role of preexisting structures during rift evolution. *Tectonics*, *21*(1), 1006. https://doi.org/10.1029/2001TC900022

Sinclair, H. D. (1997). Flysch to molasse transition in peripheral foreland basins: The role of the passive margin versus slab breakoff. *Geology*, *25*(12), 1123–1126. https://doi.org/10.1130/0091-7613(1997)025<1123:ftmtip>2.3.co;2

Strecker, M. R., Blisniuk, P. M., & Eisbacher, G. H. (1990). Rotation of extension direction in the central Kenya Rift. *Geology*, *18*(4), 299–302. https://doi.org/10.1130/0091-7613(1990)018<0299:roedit>2.3.co;2

Wirth, E. (1962). Die Erdöllagerstätten Badens. *Abhandlungen des Geologischen Landesamtes Baden-Württemberg*, *4*(5), 63–80.

Withjack, M. O., Schlische, R. W., & Olsen, P. E. (2002). Rift-basin structure and its influence on sedimentary systems. *Sedimentation in Continental Rifts—SEPM Special Publication*, *73*, 57–81.

Wrona, T., Magee, C., Jackson, C. A. L., Huuse, M., & Taylor, K. G. (2017). Kinematics of Polygonal Fault Systems: Observations from the northern North Sea. *Frontiers in Earth Science*, *5*, 101. https://doi.org/10.3389/feart.2017.00101